Experimental test of two-dimensional melting through disclination unbinding

R. A. Quinn* and J. Goree†
Department of Physics and Astronomy, The University of Iowa, Iowa City, Iowa 52242
(Received 8 November 2000; revised manuscript received 30 May 2001; published 29 October 2001)

A two-dimensional (2D) melting transition has been studied in a nonequilibrium experimental model system. The system used was a complex or dusty plasma consisting of microspheres suspended in a glow-discharge plasma, where we have mapped the topological defects during the transition. The role of the defects in the melting transition is evaluated and the arrangement of the defects in the lattice is quantified in a new way. It is found that defect density increases dramatically during the melting; at all stages the defects tend to be clustered together rather than widely dispersed; the clustering tends to take the form of chain or string-like structures. We compare these results for the defect structure with the assumptions of the popular 2D melting theory of Halperin and Nelson, rather than the predictions, as is more common.

DOI: 10.1103/PhysRevE.64.051404 PACS number(s): 82.70.Dd, 64.60.−i, 52.27.Lw, 68.35.Rh

I. INTRODUCTION

Experimental model systems have played an important role in understanding the nature of two-dimensional (2D) melting for more than a decade. Much of the current interest in 2D melting originated with the theoretical predictions of Kosterlitz, Thouless, Halperin, Nelson, and Young (KTHNY) [1–4], who suggested that phase transitions in 2D might be fundamentally different from those in 3D. The KTHNY theory inspired many simulations and experiments to test its predictions, as well as competing theories, for example, that of Chui [5]. Experimental systems that have been studied in connection with 2D melting include liquid-crystal films, adsorbed gases, electrons on liquid helium, and trapped ions (see Refs. [6] and [7]).

One successful 2D model system has been colloidal suspensions, which consist of small monodisperse spherical particles suspended in a polar solvent, such as water. The solvent acts to charge the microspheres by dissociating ions at the surface, leaving a negative surface charge which can be as high as 10^3 to 10^4 electron charges. The microspheres interact via a screened Coulomb potential and are trapped between two narrowly separated glass plates which repel the particles, thereby forming a two-dimensional structure. One striking advantage of this experimental system is that the individual particle positions can be directly imaged. This allows, for instance, defects to be identified and tracked at different stages of melting [8,9].

Here we will present results for a 2D nonequilibrium melting transition using a ''complex plasma'' model system, so-called in analogy with complex fluids. Also known as a ''strongly coupled dusty plasma,'' this system consists of charged, micron-sized particles suspended in a glow-discharge plasma. It shares many similarities with colloidal suspensions: the particles obtain a large negative charge from the suspension media, they interact via a screened Coulomb repulsion, they are trapped in one direction by a deep potential well while moving freely in the perpendicular directions, and the lattice microstructure is easily detected by direct imaging. However, complex plasmas differ from colloidal suspensions in their volume fraction and equilibration time, which are both smaller by a factor as large as 10^5.

In the present experiment we have used a complex plasma to explore changes in the microstructure of a 2D system during a melting transition to a liquid from a more highly ordered noncrystalline state that exhibits some properties of the hexatic phase. We have evaluated the correlation functions, plotted defect maps, and computed various defect statistics. Using these results we find that our observations are inconsistent with assumptions underlying a part of the KTHNY theory.

The organization of the rest of this paper is as follows. In Sec. II we review the KTHNY melting theory and two related colloidal experiments. In Sec. III we describe the complex plasma model system and the experimental setup and analysis. Then, in Secs. IV and V, we present our principle results and compare these to a part of the KTHNY theory. After presenting an empirical description of the melting process in Sec. VI, we present a brief comparison to another model in Sec. VII.

II. TWO-DIMENSIONAL MELTING THEORY AND EXPERIMENTS

A. KTHNY melting picture

Before discussing the KTHNY theory in more detail, it is important to understand how order is defined in 2D systems, and the nature of topological defects, which destroy the order. First, in a 2D solid, perfect long-range translational order does not exist at finite temperatures due to perturbations by long-wavelength phonons [10]. Instead, translational order is said to be ''quasi-long-range,'' due to the slow algebraic decay of the 2D translational correlation function [3,11]. However, perfect long-range orientational order does exist in a 2D solid, as seen in the behavior of the bond-orientational correlation function [3,11], which is constant for a solid.

In 2D, order can be destroyed by the thermal generation of two types of topological defects. First, there are dislocations, which can be interpreted as an extra half lattice row

*New address: Max-Planck-Institut für Extraterrestrische Physik, Garching, D-85748, Germany. Electronic mail: raq@mpe.mpg.de
†Electronic mail: john-goree@uiowa.edu

inserted between two existing rows. Dislocations are made of a tightly bound pair of disclinations, which are the second defect type. A disclination is defined as any lattice site having other than six nearest neighbors, because two-dimensional lattices are hexagonal. A dislocation is made of a pair of fivefold and sevenfold disclinations separated by one lattice spacing, where five and seven refer to the number of nearest neighbors of the respective disclination lattice sites.

In the KTHNY theory, the melting, or order–disorder, transition is continuous. It occurs in two steps by the generation of two types of topological defects, free dislocations and free disclinations. First, in the solid phase, a few pairs of tightly bound dislocations (disclination quadrupoles) are generated spontaneously by thermal fluctuations. As the thermal energy of the lattice is raised, these pairs can split, become widely separated, and eventually entirely disassociate [1]. The resulting free dislocations destroy the quasi-long-range translational order in the lattice; however, quasi-long-range orientational order remains [2,3]. Halperin and Nelson (HN) refer to the resulting phase as the ''hexatic'' phase. They then propose a second transition to an isotropic fluid phase as the free dislocations unbind into (pairs) of free disclinations. It is these free disclinations that destroy the remaining orientational order in the lattice. We will hereafter refer to this second phase transition as the HN hexatic-to-liquid phase transition.

For our purposes, there are two key assumptions made in the KTHNY picture of melting. One is that the overall dislocation concentration, although increasing with temperature, remains low throughout the transition. This allows the defects to be treated as a weakly interacting gas in the theory, making the dislocation unbinding calculations tractable for the solid-to-hexatic phase transition. The same low defect concentration assumption is implicitly invoked by HN for the disclination unbinding transition from the hexatic to the liquid phase, since they apply the same computational method [3]. Another assumption in the HN picture of the hexatic-to-liquid transition is that the presence and proliferation of free disclinations destroys the orientational order. In Sec. V we present results suggesting that these two assumptions are contradicted by our experimental results.

Assumptions aside, one reason that KTHNY has generated so much interest is that it makes specific predictions about the behavior of correlation functions during the melting transition (see Table I of Ref. [6], for example.) For instance, translational order is predicted to decay algebraically in the solid phase while orientational order remains long range. After dislocation unbinding, translational order is predicted to decay exponentially while orientational order decays algebraically. After disclination unbinding, both translational and orientational order are predicted to decay exponentially, with short length scales ($\sim a$, the interparticle spacing.) The degree of translational and orientational order can be measured easily in a wide variety of experiments and simulations of 2D melting by computing the pair correlation $g(r)$ and bond-orientational correlation $g_6(r)$ functions, respectively, and fitting these functions to algebraic and exponential decays [11,12].

B. Previous experiments

Many experiments have been compared to the predictions of the KTHNY theory, as reviewed in Refs. [6] and [11]. In addition, several recent experiments have explored 2D melting and the KTHNY theory for different interaction potentials. These include electric dipole interactions [13,14], magnetic dipole interactions [15], and uncharged colloidal systems [16,17]. Here we will briefly summarize two representative experiments using 2D colloidal suspensions.

Murray and Van Winkle [8] found evidence for two phase transitions with decreasing microsphere density (from solid to hexatic and from hexatic to liquid) in a series of experiments using charged submicron colloid particles in a liquid suspension. The particles were mutually repulsive and confined to a single layer between two glass plates. The plates were configured in a wedge in the direction perpendicular to the particle layer, creating a density gradient within the layer. Murray and Van Winkle imaged the particles at different locations along the wedge, corresponding to different particle densities, using an optical microscope. Using particle coordinates obtained from the images, they studied defect formation and also computed the $g(r)$ and $g_6(r)$ correlation functions.

At about the same time, Tang *et al.* [9] conducted a similar experiment, but with their particles trapped between parallel glass plates. They induced a phase transition by applying or removing a clamping force between the plates in order to vary the density of the 2D layer of particles. They used imaging and analysis techniques similar to those of Murray and Van Winkle.

The results of both colloidal experiments showed good agreement with the KTHNY predictions for the behavior of $g(r)$ and $g_6(r)$. They found long-range translational and orientational order at the highest densities, corresponding to a solid phase. At somewhat lower densities, they found shorter-range translational order, but the orientational order was still long range, matching the KTHNY predictions for the hexatic phase. Finally, at the lowest densities they found that both translational and orientational order were short range, as expected for an isotropic liquid phase.

However, the correlation functions do not tell the whole story about the role of defects in the melting transition. A fuller story is found by examining defect maps, made during various stages of the melting transition. Defect maps are two-dimensional plots showing the locations of all measured lattice sites, with non-six-fold coordinated sites marked by symbols. These maps are often made by marking the disclinations on a Voronoi diagram of the lattice. With defect maps, the spatial organization of the defects in the lattice is easily visualized.

Murray and Van Winkle concluded that their results were consistent with the assumptions of KTHNY, while Tang *et al.* inferred a more complicated melting picture. It is interesting to note that the maps in both colloidal experiments look very similar. In each case, defect concentration increases dramatically as the microsphere density is lowered, and clumping of the defects is apparent. This clumping, sometimes called ''condensation'' [18], is not predicted by KTHNY, and led Tang *et al.* to infer that the melting transi-

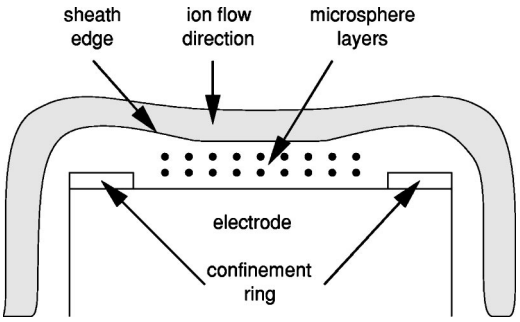

FIG. 1. Side view of an electrode showing confinement ring, sheath, and particles (microspheres). The particles are aligned in vertical chains, as sketched here.

tion is more consistent with the grain-boundary-induced melting theory of Chui [5] than with KTHNY. On the other hand, Murray and Van Winkle cite the presence of unbound disclinations to justify their support for KTHNY.

III. COMPLEX PLASMA MELTING EXPERIMENT

A. Overview

As indicated above, for our 2D model system we chose a complex plasma consisting of 6.5 ± 0.3 μm diameter, monodisperse, dielectric spheres suspended in a glow discharge plasma. Our plasma ionization was sustained by the continuous application of radio-frequency (rf) voltage to a 10 cm diameter horizontal electrode. The sheath, a natural nonneutral region in the plasma, extended from the electrode surface to a height of 3–6 mm. In the sheath there was a strong electric field that formed naturally in order to confine the plasma electrons. Within a few microseconds of insertion in the plasma, the spheres charged negatively to tens of thousands of electron charges by collecting ions and electrons. The charged particles were suspended in 2–3 layers in the electric field of the sheath, with the top layer suspended less than 1 mm below the plasma-sheath boundary. The spheres were mutually repulsive but were confined radially by a shallow ring (approximately 7 cm inner diameter) placed on the electrode. The sheath conformed to the inner edge of the ring providing the radial confining electric field (see Fig. 1).

In most circumstances the strong trap in the vertical direction locks particles into a given horizontal layer, and little vertical particle motion is observed. In contrast, the radial confinement is much weaker so that the particle motion is less restricted in the horizontal direction. A few tens of thousands of particles were trapped in the suspension. Within each cloud layer, the interparticle spacing was $a \sim 300$ μm, and the lattice arrangement was triangular with hexagonal symmetry. The same electric field that suspends the particles also accelerates ions past the particles, out of the bulk plasma and towards the electrode. Because the particles are confined by a radial potential well, they have a higher number density in the center of the suspension than in the edge [19]. Because of the compression in the center, the suspension will always have some defects, even in its most ordered state.

The interparticle potential in the system is a screened Coulomb repulsion. For monolayer complex plasmas, the potential in the horizontal direction is known from experiments to be Yukawa [20], $\phi_{\mathrm{eff}} = Q^2/a \exp(-\kappa r)$, with typical values of the particle charge $Q_p \sim 10^4$ and screening strength $\kappa = \lambda_D/a \sim 1$. Here, we have a multilayer system in which the particles' motion is mainly in the horizontal direction. Particles in the various layers are vertically aligned due to an anisotropy in the interaction potential that arises from the ion wake phenomenon [21–23]. In effect, our particles are so firmly aligned in the vertical direction that they behave like short vertical rods which move only in the horizontal direction.

The exact form of the interaction potential between the rods has not been measured experimentally, but simulations that have been reported for a bilayer system offer the best information available to characterize this potential. One approach is the fully self-consistent particle simulation of Schweigert *et al.*, Ref. [24]. They found in general that the vertically aligned particles interact through a shielded Coulomb repulsion that is modified by a small transverse attractive potential in the ambient plasma immediately downstream (in the ion flow) of an individual microsphere.

Although the nature of the mechanism which heats our particles above the temperature of the neutral gas is not important in considering our primary results, which concern the structure of the lattice, here we briefly describe what is known about the heating mechanism. The most popular model is that a mechanical instability arises in the multilayer system due to the attractive wake potential in the downstream ion flow, discussed above. The instability is suppressed at high gas pressure by gas drag on the particles [25–27]. Other mechanisms that have been evaluated include charge fluctuations, which were found to be too small and too rapid to heat the particles in our system, as explained in Ref. [28].

In the present experiment we step through a melting transition in our 2D complex plasma by reducing the argon neutral gas pressure from 500 to 140 mTorr while fixing the peak to peak electrode voltage and driving frequency at approximately 85 ± 2 V and 13.55 MHz, respectively. After each pressure step the system is allowed to settle for about 1 min so that it reaches a stable configuration. (This is the equivalent of an equilibration time for our nonequilibrium system.) A more detailed description of our apparatus is given elsewhere [29].

Although the particles in our experiment can be characterized by a kinetic temperature, they are not part of a closed system in thermal equilibrium. Power must be continuously supplied to maintain the plasma. Our entire system is comprised of the particles, the electrons and ions of the plasma, and the neutral gas. The thermal motion of the particles is determined by a balance of energy input and loss, which comes from the ions and damping on the neutral gas, respectively. Consequently, the particles acquire a distribution of energies similar to what would be observed if they were in thermal equilibrium, even though they are in fact not in thermal equilibrium with the other plasma species or the neutral gas.

Because we have a nonequilibrium system, it would be more precise to describe the phenomenon we observe as an ''order–disorder transition'' rather than a ''melting transition.'' The same thing could be said about other 2D model

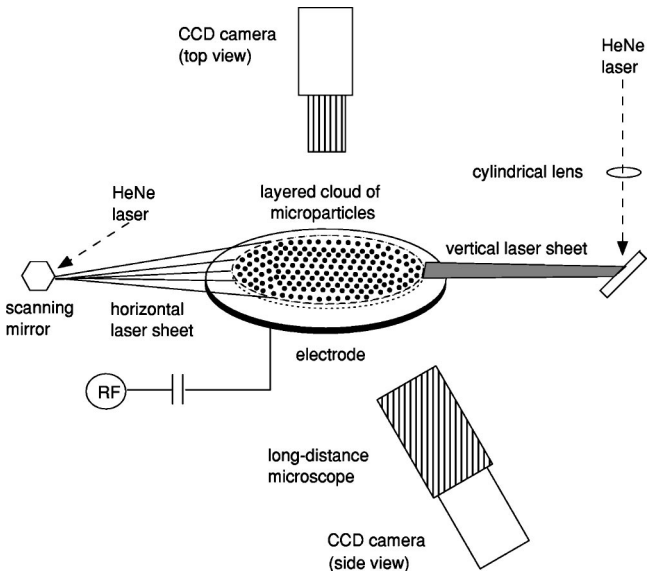

FIG. 2. Sketch of electrode, particles, and imaging optics.

systems, for example, a box of hard spheres shaken by an external source. However, for convenience and brevity, we will hereafter use the term ''melting'' instead of ''order–disorder.''

B. Analysis

Despite having multiple layers in the vertical direction, the microspheres in our experiment act as a 2D system. In order to verify this we first illuminated vertical slices of the particle cloud with a laser sheet and recorded the particle motions using a side-view camera (see Fig. 2). From the video we observed that the particles were aligned one above another in the vertical chains of 2 to 3 particles, and that each vertical chain moved as a unit in the horizontal direction. Figure 3, which shows the horizontal components of the measured trajectories of two vertically aligned particles, illustrates the two-dimensionality in two ways. First, the trajectories of the two particles track each other closely. Second, the horizontal separation of the particles is never more than about 5% of the mean interparticle spacing. The vertical motion of the particles is approximately an order of magnitude less than the horizontal.

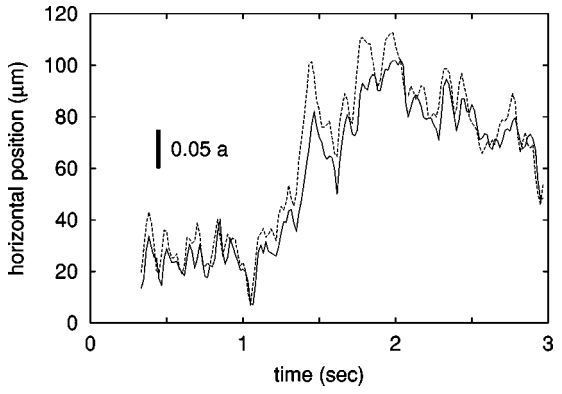

FIG. 3. Horizontal component of particle trajectories. The solid and dashed curves are the horizontal positions of two particles which are aligned in a vertical chain. The particles move together in the horizontal direction and are never separated by more than 5% of the mean interparticle spacing.

To obtain structural information about our 2D system we illuminated a horizontal slice of the particle cloud and obtained 50 snapshots, one every 4 s, of the particle locations at each pressure. Digitizing these, we found the particle locations and performed a Delauney triangulation to uniquely identify the nearest-neighbor bond network [30]. The triangulation allowed us to identify all disclinations in the lattice, defined as nonsixfold coordinated lattice sites. From these, we identified isolated disclinations and dislocations, as well as more highly clustered defects. From the particle coordinates and bond angles we computed the pair and bond-orientational correlation functions [12]. The correlation functions were averaged over all 50 snapshots.

An important question is what effect the finite and 3D extent of the system has on defects in the lattice. As mentioned above, the radial potential well confining the particles induces some defects even in highly ordered states. Another potential source of defects is the presence of one more or one less microsphere in a particular rod than in the surrounding region [31].

We also computed the particle kinetic temperature in the lattice. To do this we took 128 snapshots of the top layer of the lattice, one every 1/60 s, and obtained the individual particle trajectories. From these trajectories we computed the particle velocities and used the relation $T=m\langle v^2\rangle$ to compute the temperature. Here the angle brackets indicate an average over all particles and all times. Further details about the temperature computation are given in Ref. [32].

IV. RESULTS FOR MELTING TRANSITION

Now we present results from our experiment, showing that a melting transition takes place as we adjust neutral gas pressure. Our results are consistent with previous melting experiments using complex plasmas [33,34], the structure becomes more disordered as the gas pressure is reduced.

The first evidence that a transition is taking place can be seen in Figs. 4 and 5, which show the pair correlation function $g(r)$ and bond-orientational correlation function $g_6(r)$, respectively, as a function of neutral gas pressure. Using the method of Ref. [12], these data have been fit, in the case of $g(r)$, with a series of exponentials at the ideal lattice sites, suppressed by an exponential envelope yielding a translational correlation length ξ. The function $g_6(r)$ has been fit by a decaying exponential function only to yield an orientational correlation length ξ_6, as is frequently done in colloidal melting experiments [11]. Figures 4 and 5 show the decrease in translational and orientational order, respectively, as pressure is decreased. The dependence of the particle kinetic temperature T on pressure is shown in Fig. 6.

Additional evidence for the melting transition is presented in Fig. 7, which shows the fit correlation lengths ξ and ξ_6, normalized by interparticle spacing a, as a function of gas pressure. Note especially the strong decrease in ξ_6, indicating a rapid loss of orientational order, as the gas pressure is

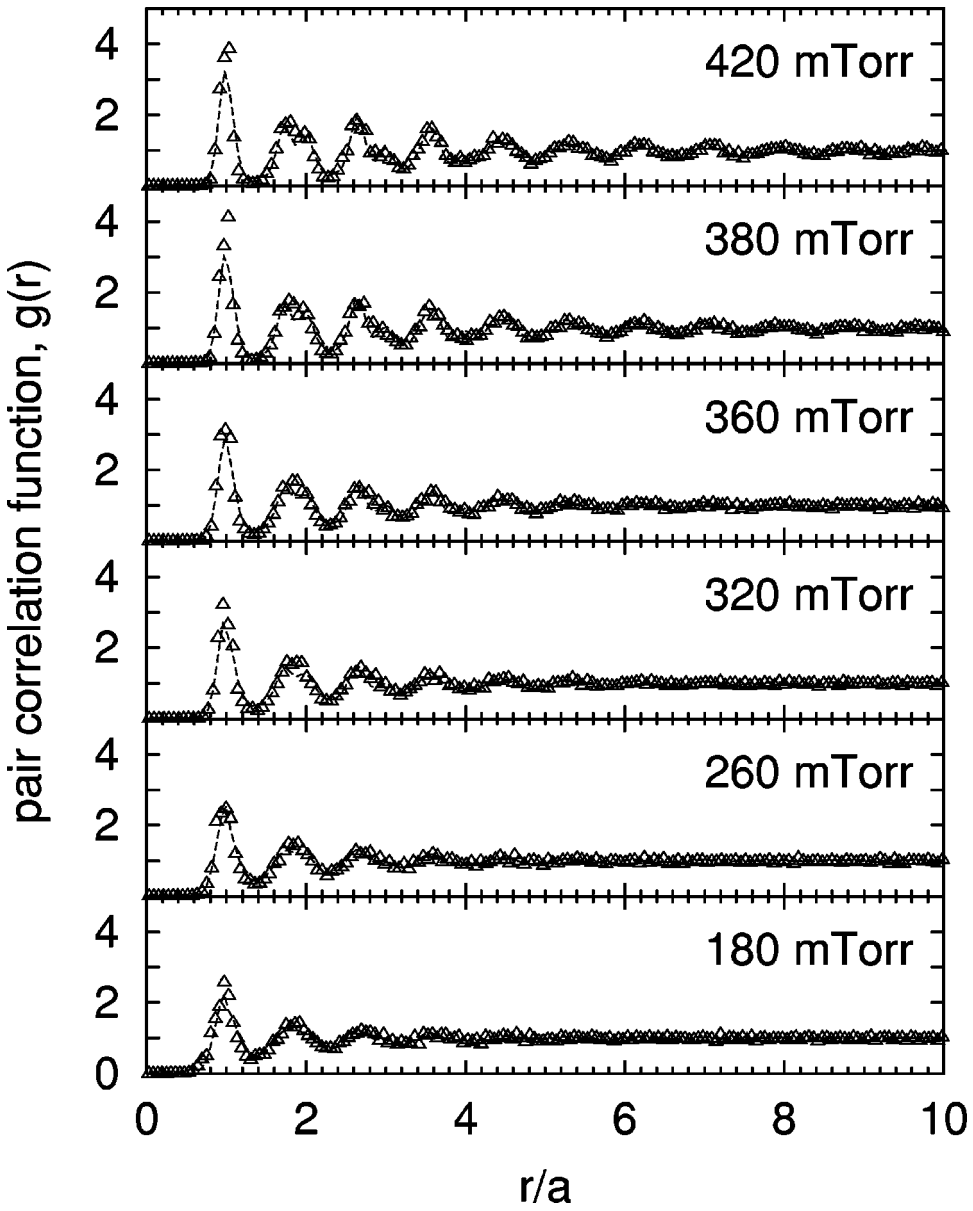

FIG. 4. Pair correlation function $g(r)$ as a function of gas pressure. Experimental data are shown with symbols while the dashed line is a fit with exponential suppression, yielding a translational correlation length, ξ. A melting transition is observed, with the highest order at the highest pressure.

reduced below 420 mTorr. For higher gas pressures, the system is essentially independent of gas pressure, so that gas pressure is primarily useful as a control parameter below 420 mTorr.

The power-law fit coefficients η_6 to $g_6(r) \propto r^{-\eta_6}$, shown in Fig. 8, provide a connection between our melting transition and the HN prediction. Recall that HN predict a hexatic phase for $\eta_6 < 0.25$, and a liquid phase for larger values of η_6. In Fig. 8 we see that below about 370 mTorr η_6 increases rapidly above the critical value. At approximately the same pressure, referring back to Fig. 7, the magnitude of ξ_6 rapidly approaches that of ξ, matching another HN prediction for the appearance of a liquid phase. Thus the behavior of the correlation functions in our experimental melting transition agree with these relevant HN predictions and, from this point of view, the hexatic-liquid transition occurs at ~ 370 mTorr. However, it is useful to note that the order in the system continues to decrease below this pressure. As indicated above, many experiments and simulations, in colloidal as well as complex plasma suspensions, have yielded similar observations for the correlation functions.

V. TEST OF HN ASSUMPTIONS

In the previous section we showed that our measured translational and orientational correlation functions are consistent with a melting transition and with certain HN predictions. However, the two key structural assumptions underlying the HN theory are not supported by the data. Recall that these assumptions are that defect concentration is low during

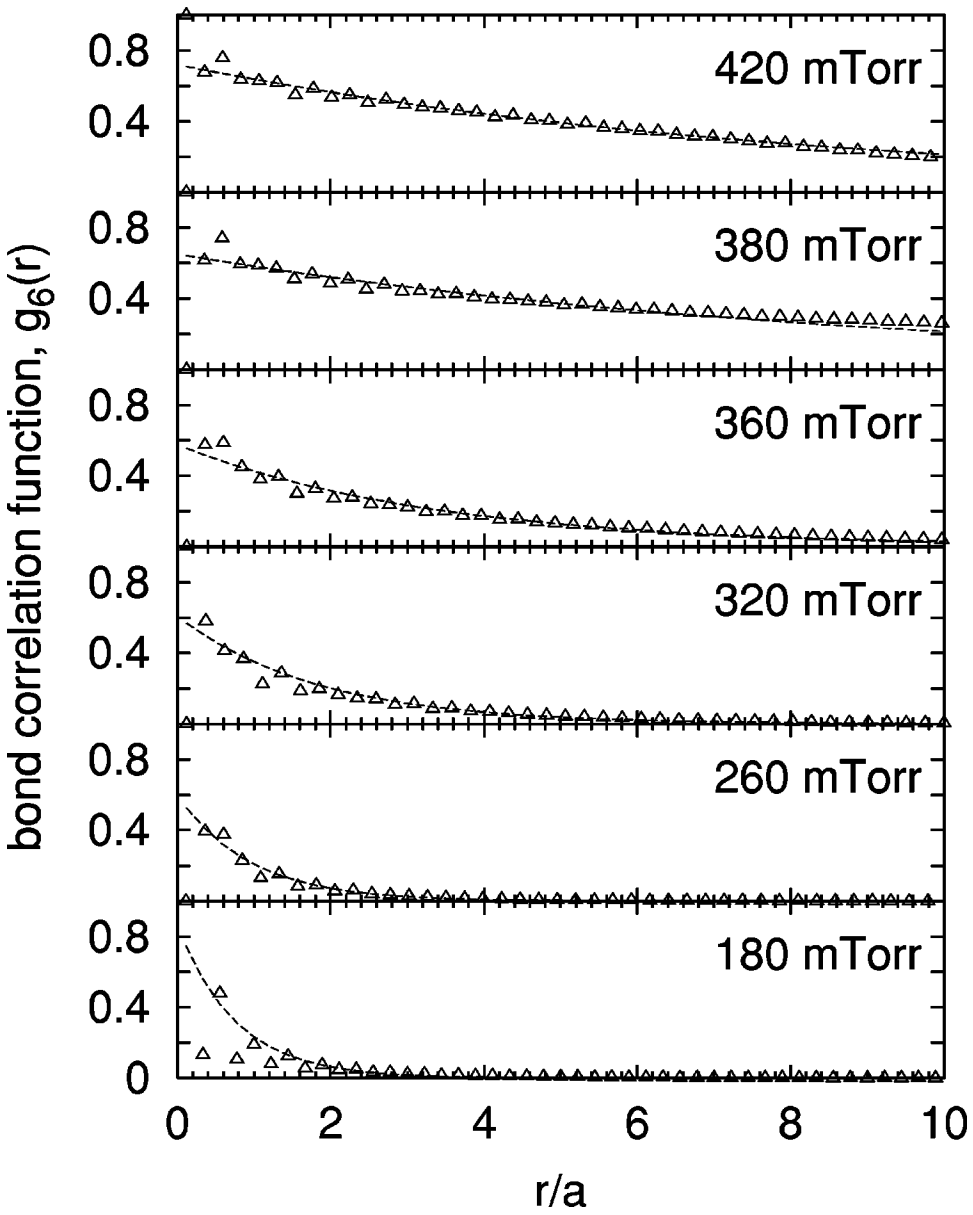

FIG. 5. Bond orientational correlation function $g_6(r)$ as a function of gas pressure. Experimental data are shown with symbols while the dashed line is a fit with exponential suppression, yielding an orientational correlation length, ξ_6. At 320 mTorr and lower pressures $g_6(r)$ decays rapidly, indicating a loss of orientational order.

the transition, and that the destruction of orientational order is due to free disclinations. Both assumptions are contradicted by our experiment, as we will now show.

In analyzing the HN assumptions we focus on the organization of defects in the lattice. Defect maps, shown in Fig. 9, present a good visual picture of the defect behavior during the melting transition. Figure 9 shows four representative defect maps, at different disclination concentrations, representing progressively lower ordered states. In these maps, triangles mark fivefold disclinations, squares mark sevenfold disclinations, and stars mark all other disclinations. Nondefect lattice sites are shown as points and the map is overlayed with the Voronoi diagram. Adjacent triangles and squares surrounded by nondefected lattice sites are isolated dislocations. Any area where three or more adjacent triangles or squares adjoin is a condensed defect region, and we refer to the constituent disclinations as ''condensed defects.''

Several general observations can be made simply by looking at the defect maps in Fig. 9. For instance, at the lowest disclination concentration in Fig. 9(a), the defects tend to be arranged in short condensed strings and isolated dislocations. Based on the corresponding correlation functions for this disclination concentration, this state could be identified as the ''hexatic phase.'' In the same sense, Fig. 9(b) would represent the first state after melting into the liquid phase. Here, a few free disclinations are present, but they do not appear to be the dominant cause of the loss of order, as discussed below. It is also interesting to note that as the disclination concentration increases in Figs. 9(b)–9(d), the stringy regions grow longer and thicker, and the concentration of iso-

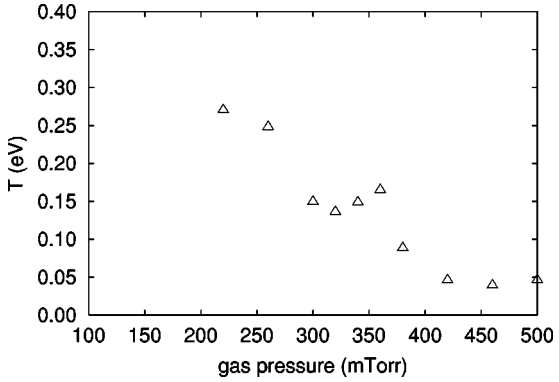

FIG. 6. Particle kinetic temperature T versus neutral gas pressure.

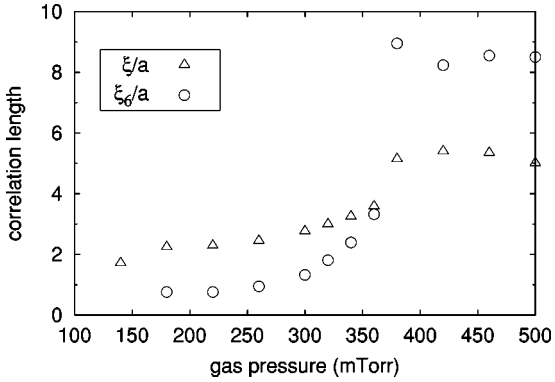

FIG. 7. Correlation lengths ξ and ξ_6, normalized by a, versus pressure. Note the rapid decrease in orientational order, as measured by ξ_6/a, as pressure is decreased below 420 mTorr. For pressures above 420 mTorr the order is insensitive to neutral gas pressure.

lated dislocations decreases. At the same time, the concentration of isolated disclinations does not appear to increase.

Focusing more closely on the role of isolated disclinations, it appears that they cannot be responsible for the destruction of order in the lattice. There are two reasons for this conclusion: isolated disclinations are never widely separated from other highly defected regions, and they are rare, as we will show below. As an example of an isolated disclination, we have identified one in Fig. 9(d) using tick marks to show its location. Note that 5 out of 16 of its next nearest neighbors are members of condensed chains of defects. Examining the area slightly farther from the isolated disclination we observe that it is almost completely surrounded by chains of condensed defects. Reviewing 20 similar maps we found that every free disclination had at least one chain or group of condensed defects nearby, within $\sim 2a$. On average, free disclinations were found to have three condensed disclinations within a radius of $\sim 2a$. These nearby chains would tend to screen any long-range effects of the free disclinations.

The assumption that free disclinations destroy the orientational order during the transition is also contradicted in Fig. 10. Figure 10 is a stacked bar plot showing the relative concentrations of isolated dislocations, isolated disclinations, condensed defects, and sixfold coordinated particles as a function of pressure during the melting transition. The concentration of isolated disclinations does increase slightly but is always very small in magnitude ($<0.7\%$). The condensed defect concentration increases from 10% to 47% during the same transition, suggesting that condensed defects rather than disclinations dominate the physics of the transition. Additionally, the concentration of condensed defect regions is much higher than that of isolated defects. Thus, even in the most highly ordered states, there are relatively few defects in the lattice that satisfy the HN assumption of low defect density.

The total disclination concentration serves as a good measure of order or disorder. This is shown in Fig. 11, which is a semilog plot of $g(r)$ and $g_6(r)$ versus total disclination concentration. This figure shows that translational and orientational order are reduced exponentially with disclination concentration. Figures 4–10 show the phenomenological behavior of our system. Having established that we can control the order in the system and the number of defects by varying the neutral gas pressure, we will hereafter use the concentration of disclinations rather than the gas pressure as the independent variable for parametrizing our data. The main reason for doing so is that the disclination concentration is more directly and physically connected to the degree of order in the system, as we have just seen. This can also be seen in Fig. 12, which shows T versus the disclination concentration.

VI. EMPIRICAL MELTING DESCRIPTION

In this section we would like to build up a more accurate, albeit empirical, picture of what is happening during our melting transition. In order to do this we will refer to the defect maps presented in Fig. 9. Based on these maps, we introduce a new derived parameter, the defect condensation parameter S, which characterizes the organizational structure of the defects themselves.

The arrangements of defects shown in Fig. 9 are interesting and can be quantified to some degree by computing S. This parameter is shown in Fig. 13, plotted versus disclina-

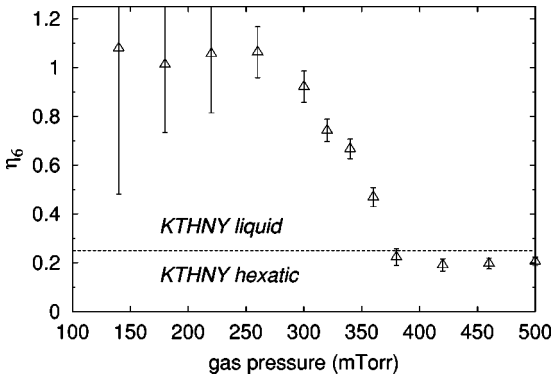

FIG. 8. Plot of $g_6(r)$ power-law fit coefficient η_6 versus pressure. Halperin and Nelson (HN) predict a threshold $\eta_6<0.25$ for the hexatic phase, while higher values of η_6 indicate a liquid phase. In our experiment $\eta_6<0.25$ for pressures greater than about 370 mTorr. This and the previous three plots demonstrate that the gas pressure is a useful control parameter that allows the experimenter to drive the lattice through a melting transition.

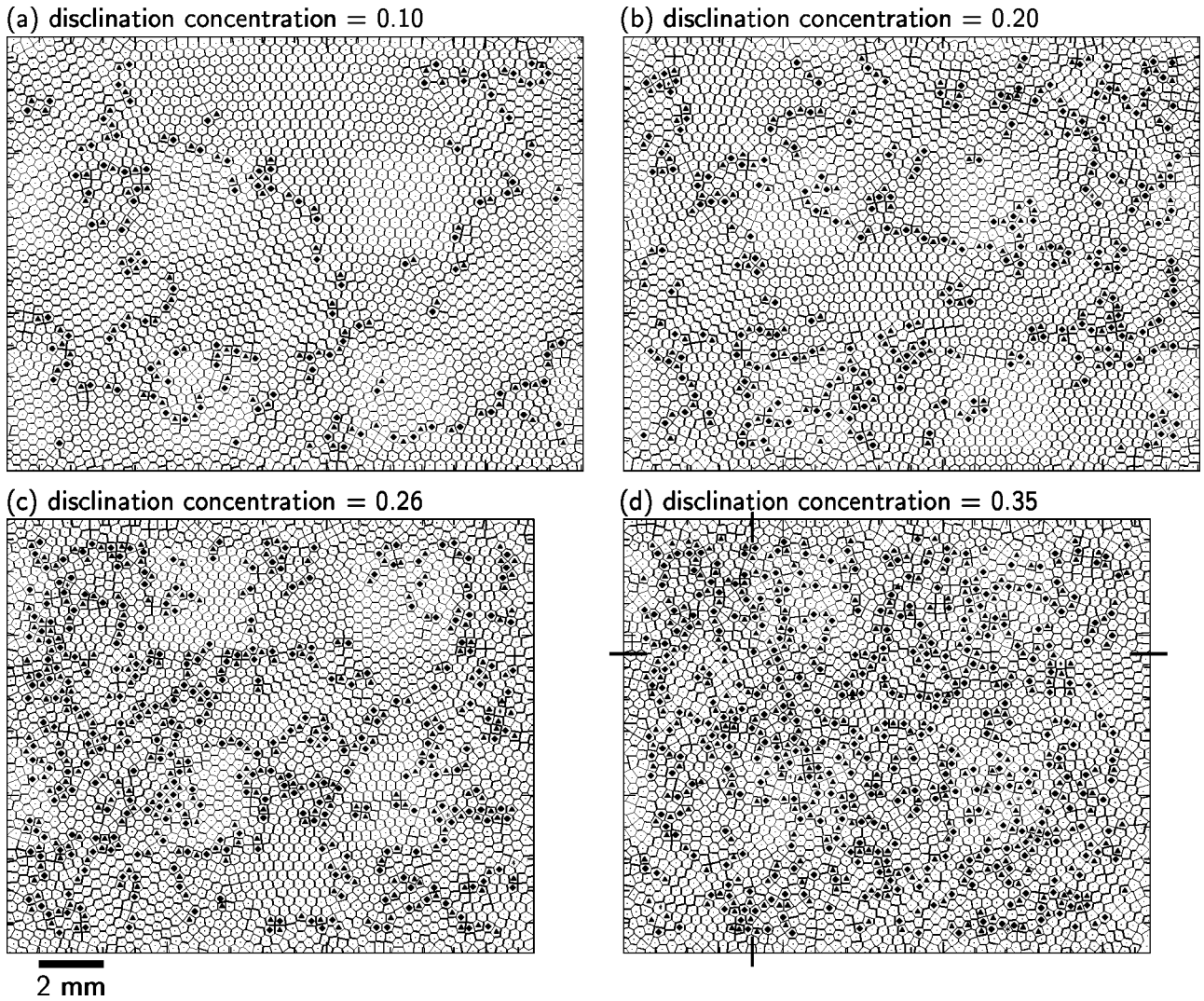

FIG. 9. Defect maps at four disclination concentrations. Triangles represent fivefold disclinations, squares represent sevenfold disclinations, and other nonsix-fold coordinated lattice sites are marked with stars. Note that at all concentrations the defects tend to be condensed into ''stringy'' regions. At higher concentrations, as in (c) and (d), the stringy regions become thicker and interconnect. The tick marks in panel (d) indicate the position of a representative isolated disclination.

tion concentration. The parameter S is the average number of a disclination's nearest neighbors that are also disclinations. If all defects were isolated disclinations, S would be zero. If all were isolated dislocations, S would be unity. If all disclinations were arranged in strings, S would approach two, and larger values of S indicate a higher degree of defect clumping. The values that S takes on for different defect configurations are given in Table I.

Also shown in Fig. 13 is S computed for a hypothetical noninteracting dislocation gas. This ''gas'' consists of disclination pairs placed randomly on a perfect triangular lattice. This illustrates how S might be expected to behave in a system having only noninteracting, isolated dislocations.

According to Fig. 13, the defect arrangements in the experiment are mostly string-like. It also shows that they are more stringy than they are in a dislocation gas. The dislocation gas data show that S increases with disclination density due to random groupings of dislocations. In comparison, S computed for the experimental data is closer to the value 2 (see Table I), indicating that the real disclinations are more likely to be arranged in stringy structures, at all defect concentrations.

VII. GRAIN BOUNDARY INDUCED MELTING

An alternative to KTHNY is the grain-boundary induced melting theory of Chui [5]. This frequently cited theory suggests that grain boundaries spontaneously form in two-dimensional crystals and drive a first-order phase transition into a liquid phase. According to Chui, since grain boundaries consist of an array of dislocations, the generation of grain boundaries implies a ''dramatic increase in the total number of dislocations'' [5]. Chui also addresses the issue of a hexatic phase, taking the definition from KTHNY, i.e., that the hexatic is a phase displaying short-range translational order and quasi-long-range orientational order. He claims that a hexatic phase can occur only if grain boundaries appear in bound pairs of opposite Berger's vectors. In this case,

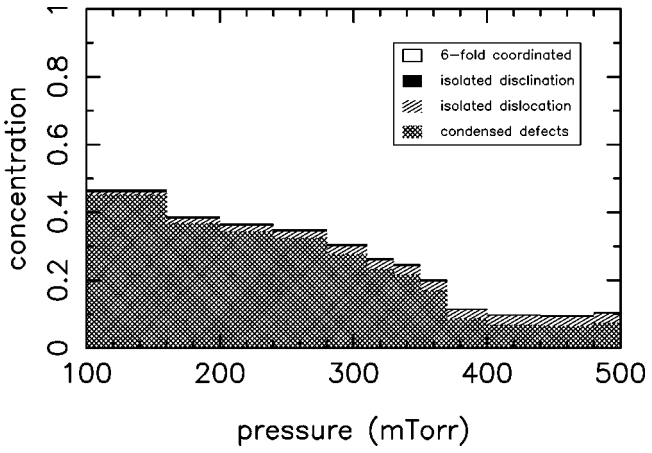

FIG. 10. Defect and sixfold coordination concentrations versus pressure. Notice that the concentration of condensed defects increases dramatically while the concentration of isolated defects either decreases (dislocations) or increases only slightly (disclinations). Condensed defects here are defined to be three or more adjacent disclinations.

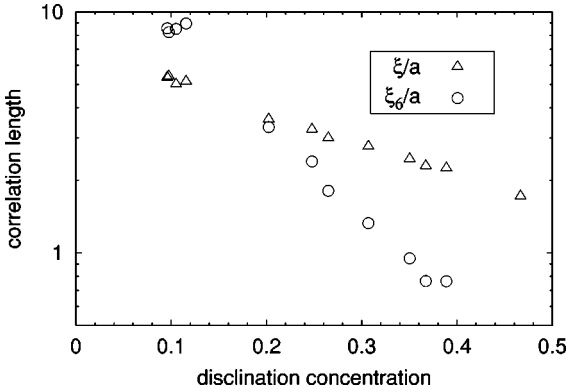

FIG. 11. Correlation lengths ξ/a and ξ_6/a versus disclination concentration.

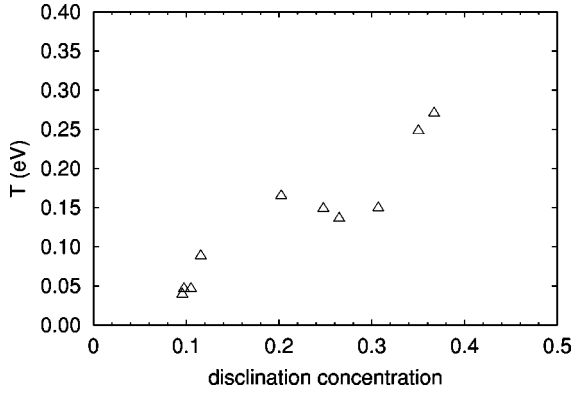

FIG. 12. Particle kinetic temperature T versus disclination concentration.

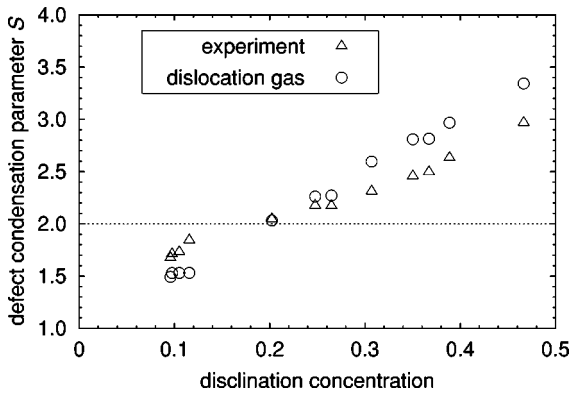

FIG. 13. Defect condensation parameter S versus disclination concentration. The parameter S is the average number of a disclination's nearest neighbors that are also disclinations. For comparison, we also show S as a function of disclination concentration for a hypothetical ''dislocation gas'' consisting of disclination pairs scattered randomly on a hexagonal lattice.

every time one crosses a grain boundary, e.g., while computing $g_6(r)$, the orientation of the crystal changes, but then quickly changes back as the other grain boundary in the pair is crossed. In this scenario, translational order is destroyed by the grain boundaries, but orientational order is preserved. However, Chui finds that bound pairs of grain boundaries cannot exist above the melting temperature, and that a hexatic phase should not be found.

Our results show some qualitative agreement with Chui's theory. At the lowest disclination concentrations, the stringy structures that we observe appear to be grain boundaries, as in Fig. 9(a). These ''grain boundaries'' proliferate and interconnect during the melting transition, and we see a significant increase in the total number of disclinations. However, correlation functions for our most highly ordered states are consistent with those expected for a hexatic phase and we find no conclusive evidence of grain boundary pairing in our experiment. It should also be noted that a true test of Chui's theory requires an initial crystalline state having very low defect density which we were unable to obtain in this experiment, as discussed above.

VIII. CONCLUSION

In this paper we have established that experimental complex plasma suspensions are a useful model system for studying 2D order–disorder (melting) phase transitions. Using such a plasma, we examined a melting transition in detail

TABLE I. S is a defect condensation parameter defined as the average number of a disclination's nearest neighbors that are also disclinations. It takes on the following values for these defect arrangements.

If S	$=0$	isolated disclinations
	$=1$	isolated dislocations
	$=2$	long disclination strings
	>2	clumps or thickened strings

and found that two central assumptions of the HN hexatic-to-liquid transition theory are contradicted in our experiment. First, we found that the disclinations were condensed in string-like regions throughout the experiment, contradicting the assumption that disorder in the liquid state is primarily due to free disclinations. Second, we found that isolated disclinations do not appear to be the cause of the loss of orientational order in our system. Several pieces of evidence suggest that this isolated disclination concentration is low for all conditions, condensed disclination concentration rises rapidly during melting, and isolated disclinations are always surrounded by condensed chains of disclinations within a distance of two interparticle spacings.

The presence of these condensed chains lead to an interesting empirical picture of the 2D melting transition. In the most highly ordered examples of this experiment, long thin strings of defects thread the lattice. As order proceeds to disorder during the transition, more defect chains appear, becoming thicker and more entwined. As an additional conclusion, our quantitative method of characterizing the shape of condensed defects shows that they are always more stringy than would be expected for a random distribution of dislocations.

In seeming contradiction with this empirical picture of the melting transition, the $g(r)$ and $g_6(r)$ correlation functions are found to be consistent with some of the HN theory's predictions. From this one might reasonably conclude that a hexatic–liquid phase transition has taken place in our experiment. However, the correlation functions represent spatial averages that can include domains of crystalline order as well as liquid-like domain walls (condensed defect strings.) Additionally, different crystal domains can generally have different lattice orientations. Thus, because of spatial averaging, correlation functions can mimic the behavior predicted for the HN transition, even though an examination of the underlying structure suggests otherwise.

Finally, we would like to point out that our defect maps and correlation function results are qualitatively quite similar to results obtained in many previous 2D colloidal experiments, including screened-Coulomb [8,9], electric dipole [13,14], and magnetic dipole [15]. Regarding the behavior of the correlation functions, all of these systems exhibit good agreement with the predictions of KTHNY. Our main emphasis here is not to test the predictions of KTHNY, but rather the assumptions underlying that theory. We did this by analyzing the structure of the lattices in terms of the distribution of defects.

ACKNOWLEDGMENTS

We thank D. Samsonov, I. V. Schweigert, and V. A. Schweigert for helpful discussions. This work was supported by NASA and the National Science Foundation.

[1] J. M. Kosterlitz and D. J. Thouless, J. Phys. C **6**, 1181 (1973).
[2] B. I. Halperin and D. R. Nelson, Phys. Rev. Lett. **41**, 121 (1978).
[3] D. R. Nelson and B. I. Halperin, Phys. Rev. B **19**, 2457 (1979).
[4] A. P. Young, Phys. Rev. B **19**, 1855 (1979).
[5] S. T. Chui, Phys. Rev. B **28**, 178 (1983).
[6] K. J. Strandburg, Rev. Mod. Phys. **60**, 161 (1988).
[7] J. J. Bollinger *et al.*, Phys. Plasmas **7**, 7 (2000).
[8] C. A. Murray and D. H. Van Winkle, Phys. Rev. Lett. **58**, 1200 (1987).
[9] Y. Tang, A. J. Armstrong, R. C. Mockler, and W. J. O'Sullivan, Phys. Rev. Lett. **62**, 2401 (1989).
[10] N. D. Mermin, Phys. Rev. **176**, 250 (1968).
[11] C. A. Murray, in *Bond Orientational Order in Condensed Matter Systems*, edited by K. J. Strandburg (Springer-Verlag, New York, 1992), Chap. 4.
[12] R. A. Quinn *et al.*, Phys. Rev. E **53**, R2049 (1996).
[13] R. E. Kusner, J. A. Mann, J. Kerins, and A. J. Dahm, Phys. Rev. Lett. **73**, 3113 (1994).
[14] R. E. Kusner, J. A. Mann, and A. J. Dahm, Phys. Rev. B **49**, 9190 (1994).
[15] K. Zahn, R. Lenke, and G. Maret, Phys. Rev. Lett. **82**, 2721 (1999).
[16] A. H. Marcus and S. A. Rice, Phys. Rev. Lett. **77**, 2577 (1996).
[17] A. H. Marcus and S. A. Rice, Phys. Rev. E **55**, 637 (1997).
[18] M. A. Glaser and N. A. Clark, in *Advances in Chemical Physics*, edited by I. Prigogine and S. A. Rice (Wiley, New York, 1993), Vol. LXXXIII, Chap. Melting and liquid structure in two dimensions.
[19] W.-T. Juan *et al.*, Phys. Rev. E **58**, R6947 (1998).
[20] U. Konopka, G. E. Morfill, and L. Ratke, Phys. Rev. Lett. **84**, 891 (2000).
[21] F. Melandsø and J. Goree, Phys. Rev. E **52**, 5312 (1995).
[22] O. Ishihara and S. V. Vladimirov, Phys. Plasmas **4**, 69 (1997).
[23] A. Melzer, V. A. Schweigert, and A. Piel, Phys. Rev. Lett. **83**, 3194 (1999).
[24] V. A. Schweigert, I. V. Schweigert, V. Nosenko, and J. Goree (unpublished).
[25] A. Melzer *et al.*, Phys. Rev. E **54**, R46 (1996).
[26] V. A. Schweigert *et al.*, Phys. Rev. E **54**, 4155 (1996).
[27] F. Melandsø, Phys. Rev. E **55**, 7495 (1997).
[28] R. A. Quinn and J. Goree, Phys. Rev. E **61**, 3033 (2000).
[29] J. B. Pieper, J. Goree, and R. A. Quinn, J. Vac. Sci. Technol. A **14**, 519 (1996).
[30] S. Fortune, Algorithmica **2**, 153 (1987).
[31] I. V. Schweigert, V. A. Schweigert, A. Melzer, and A. Piel, Phys. Rev. E **62**, 1238 (2000).
[32] R. A. Quinn and J. Goree, Phys. Plasmas **7**, 3904 (2000).
[33] A. Melzer, A. Homann, and A. Piel, Phys. Rev. E **53**, 2757 (1996).
[34] H. M. Thomas and G. E. Morfill, J. Vac. Sci. Technol. A **14**, 501 (1996).